Mode-locked and tunable 3.5 µm fiber laser using an acousto-optic modulator

Ori Henderson-Sapir, *Member, IEEE*, Nathaniel Bawden, Antreas Theodosiou, *Member, IEEE*, Matthew R. Majewski, Kyriacos Kalli, *Member, IEEE*, Stuart D. Jackson, *Fellow, IEEE,* and David J. Ottaway, *Member, IEEE*

***Abstract*—A mode-locked, dual-wavelength pumped 3.5 µm fiber laser using frequency shifted feedback utilizing an acousto-optic modulator is reported. Pulses of 3.8 ps with 9.7 nJ were obtained at a repetition rate of 37.75 MHz. The resulting peak power is 2.55 kW. An electronically wavelength swept, mid-IR interrogator is built to characterize a mid-IR fiber Bragg grating.**

***Index Terms*—**

I. Introduction

MODE-LOCKED fiber lasers operating in the 2.8 µm to 3.5 µm wavelength range have undergone continued performance improvements in recent years, motivated by applications in atmospheric sensing [1], polymer processing [2] and medicine [3]. The wavelength band of 3.5 µm has undergone a renaissance in interest since dual wavelength pumping was shown to be an efficient and effective pumping mechanism for this band [4]. Various demonstrations of mode-locking based on different techniques have been achieved including frequency-shifted-feedback (FSF) [5], saturable absorbers [6] and non-linear polarization rotation (NPR) [7]. These three techniques resulted in different time scales of pulse duration: tens of picoseconds, few picoseconds and sub-picosecond, respectively. The various methods for generating mode-locking at the 3.5 µm band and their relative time scales are discussed below, starting with generation using saturable absorbers.

A growing number of saturable absorber types have been used to demonstrate pulsed operation (Q-switched) in 3.5 µm fiber lasers, see I. These include 2D materials such as black phosphorous [6] (2 µs), carbon nanotubes [8], antimonene [9] (3.6 µs) and Fe^{2+}:ZnSe [10] (1.8 µs) in addition to semiconductor saturable absorbers (SESAMs) [11]–[13] (2.5–2.9 µs). Employing these saturable absorbers resulted in Q-switching in all cases, however mode-locked operation proved more elusive since only black phosphorous [6], a SESAM [12] (14.5 ps) and carbon nanotubes [8] (1.7 ps) have produced mode-locked operation. Malouf et al. [14] showed strong two-photon absorption in graphene becomes dominant at high intensities generating high resonator losses, which are likely to be detrimental to lasing at 3.5 µm. This result supported our own work which was unsuccessful in reaching mode-locking threshold using graphene in a 3.5 µm fiber laser system. It is potentially possible that other saturable absorbers might provide a route to mode-locking at the 3.5 µm, or display similar effects to graphene dictating favouring relatively long pulses or not reaching mode-locking threshold at all.

The shortest duration mode-locked pulses in the 3.5 µm band have been generated using NPR [7] (580 fs), however the need to create a free space ring with multiple elements makes NPR implementation challenging in the low gain 3.5 µm system. Shorter pulse formation is likely with improved dispersion control and increased pump availability [7].

FSF achieves mode-locked like operation by incorporating a frequency shifting element such as an acousto-optical modulator (AOM) or an acousto-optical tunable filter (AOTF) in the resonator. The frequency shift that this introduces is balanced by self phase modulation caused by the intensity dependant Kerr effect. If bandpass filtering is present in the resonator, short pulsed operation is favoured.

In a previous work we have shown that FSF is a suitable technique for achieving mode-locked like pulses [5]. In this case a resonator with an intracavity AOTF produced pulses with durations of 53 picoseconds. Due to the AOTF's relatively long interaction length, only a narrow band of frequencies that satisfy the phase-matching condition are diffracted [15], limiting the achievable spectral bandwidth and hence the long pulse duration operation. An AOTF has a narrower spectral transmission bandpass compared with an AOM and hence shorter duration operation using FSF has been shown previously using an AOM in a holmium-praseodymium system operating around 3 µm [16]. Other spectrally limiting effects such as atmospheric absorption at the 3 µm band in the resonator can also cause profound limitation on pulse formation. [17].

In the 3.5 µm band atmospheric absorption due to water

This work was supported in part by the US Air Force Office of Scientific Research award FA-9550-20-1-0160 and in part by the University of Adelaide.

This work was performed, in part, at the Opto Fab node of the Australian National Fabrication Facility supported by the Commonwealth and SA State Government.

O. Henderson-Sapir, N. Bawden and D. J. Ottaway are with the Department of Physics and Institute of Photonics and Advanced Sensing, The University of Adelaide, Adelaide, SA, Australia. Corresponding author: ori.henderson-sapir@adelaide.edu.au.

O. Henderson-Sapir is also with Mirage Photonics, Oaklands Park, SA, Australia.

A. Theodosiou is with the Lumoscribe Ltd., 8310 Paphos, Cyprus, and also with the Photonics and Optical Sensors Research Laboratory, Cyprus University of Technology, 3036 Limassol, Cyprus (e-mail: theodosiou.antreas@lumoscribe.com).

K. Kalli is with the Photonics and Optical Sensors Research Laboratory, Cyprus University of Technology, 3036 Limassol, Cyprus (e-mail: kyriacos.kalli@cut.ac.cy).

M. R. Majewski and S. D Jackson are with MQ Photonics, School of Engineering, Faculty of Science and Engineering, Macquarie University, North Ryde, NSW, Australia.

Manuscript received August xx, 2021; revised August xx, 2021.

TABLE I
REPORTED Q-SWITCHING AND MODE LOCKING PULSE WIDTHS AT THE 3.5 µm BAND.

Pulse generation method	Q-switched pulse width [µs]	Mode-locked pulse width [ps]	Ref.
Black Phosphorous	2	3.8 *	[6]
SESAM	2.47	–	[11]
SESAM	–	18.1	[12]
SESAM	–	14.8	[13]
Carbon nanotubes	–	1.7	[8]
Antimonene	3.6	–	[9]
Fe^{2+}:ZnSe	1.8	–	[10]
NPR	–	0.580	[7]
AOM (germanium)	0.32	–	[18]
FSF (TeO_2 AOTF)	0.435	–	[19]
FSF (TeO_2 AOTF)	–	53	[5]
FSF (TeO_2 AOM)	–	3.8	This work

– When value is left blank, the associated behaviour was not reported.
* These pulse widths were not directly measured and were not reported in this reference. The value presented here is a lower bound inferred from the reported spectral width, assuming transform limited pulses.

vapour and CO_2 is minimal compared with its magnitude at the 2.8–3.0 µm band and is expected to play a reduced role in limiting the spectral bandwidth of the generated pulses in resonators which are not excessively long [17]. Therefore, it is expected that FSF based mode-locking operation of lasers in this band will be entirely limited by the gain-bandwidth of the gain species as well as the spectral limitations induced by the frequency-shifting optical element.

The FSF based method also opens the door to electronic wavelength control of the laser output. Rapid Wavelength tuning of a mid-IR laser light sources is advantageous in many aspects and applications. These include for instance, increased absorption and sensitivity in trace gas sensing [20], better resolution and selectivity in polymer processing [21] or increasing contrast when investigating biological samples [22]. The electronic wavelength tunability presented here has a significant advantage over lasers with mechanically tuned diffraction grating-stabilization which requires mechanical orientation of the grating with tuning rates on the order of tens to hundreds of milliseconds. Fast wavelength tunability is of great interest in LIDAR based applications [23] as well or in other applications which require fast throughput as in atmospheric sensing [24] and breath analysis [3].

In this work, we expand on our previous FSF work with an AOTF and replace it with an AOM demonstrating over an order of magnitude shorter mode-locked pulses in the 3.5 µm band. In addition, we demonstrate by changing the drive frequency of the AOM we can electronically sweep the wavelength of operation of the laser over 50 nm. To the best of our knowledge this is the first demonstration of an electronic-only wavelength tuning of a fiber laser in the mid-IR which does not involve using an AOTF. As a proof of concept, the electronically tunable source is then used as a mid-IR fiber Bragg grating (FBG) interrogator, the first such demonstration in the mid-IR to the authors' knowledge.

II. MODE-LOCKED LASER

Mode-locking behaviour using frequency shifted feedback (FSF) requires the laser resonator to contain a spectral filter and a non-linear element in addition to a frequency shifting element [25]. Each round trip light is amplified and frequency shifted so long as its wavelength remains within the linewidth of the filtering element. This behaviour is akin to the behaviour of a seeded laser amplifier rather than a laser resonator (Sabert [26]). Eventually, the wavelength is shifted sufficiently so it goes beyond the spectral boundaries of the filtering element. With sufficient gain this phenomenon can result in continuous wave (CW) operation with a linewidth that is larger than that of an ordinary laser. This is due to the lack of regenerative amplification of longitudinal modes with a resulting mode-less structure. Further insight into the creation of CW lasing in an FSF system is provided by Littler [27].

Sabert et al. showed that pulsed operation can be sustained if the seeding of the amplified signal is by laser modes that maintain a phase and amplitude relation, therefore creating feedback [26]. Neighboring spectral components will share phase, resulting with a pulse in the time domain. Once a clear pulse is created, self phase modulation due to the Kerr effect will push the wavelength of light back to within the bounds of the filtering element thereby counteracting the frequency shift. This trend will favour short pulse operation in contrast to CW.

A. Experimental setup

The experimental setup for our mode-locked source is shown schematically in Fig. 1. It is similar to the setup used in [5] with an AOM replacing the AOTF. Note that in the current work, the AOM operates in a continuous mode, where the diffracted beam is not switched on and off. The diffracted beam is always on, resulting in a fraction of the circulating power always being diffracted and gaining a frequency shift, while the reminder of the power continues through the non-diffracting port of the AOM, acting as the laser output. Following the dual-wavelength pumping scheme [4], the two pumps are free-space combined on a dichroic mirror and eventually focused into the gain medium fiber using an anti-reflective coated, custom ZnSe aspheric lens with a 0.5 NA and 9 mm focal length. The two pumps are a 30 W, 977 nm multi-mode fiber coupled diode (LIMO HLU30F200-977), which is launched into the cladding of the gain fiber. A 1973 nm Tm^{3+} doped silica fiber laser beam (Mirage Photonics TFL-2000), is launched into the core of the fiber.

The linear resonator uses a 2.3 m long 1 mol.% Er^{3+}:ZrF_4 fiber (Le Verre Fluoré) as the gain medium. This double-clad fiber has a 16.5 µm diameter core with a 0.12 NA at 3.5 µm and a 240/260 µm double-truncated circular inner cladding. The group velocity dispersion β_2 of the fiber used is $(-0.191 \pm 0.009) \times 10^{-24}\,\mathrm{s^2\,m^{-1}}$, as was found in [7]. Both ends of the gain medium fiber are polished flat. A highly reflective (HR) mirror at the 3.5 µm band is butted against the distal end of the fiber.

Intra-cavity the 3.5 µm laser light is reflected from the 45° dichroic mirror at the pump input end. It then passes through a half-wave plate before being incident on a tellurium-dioxide

AOM (Gooch & Housego 33041- 20-2.5-2.65/2.9-TeO2-TB-SMF). An HR mirror retro-reflects the AOM diffracted order, completing the laser resonator and the non-diffracted beam acts as the laser output. The length of the free space section of the laser is approximately 0.5 m.

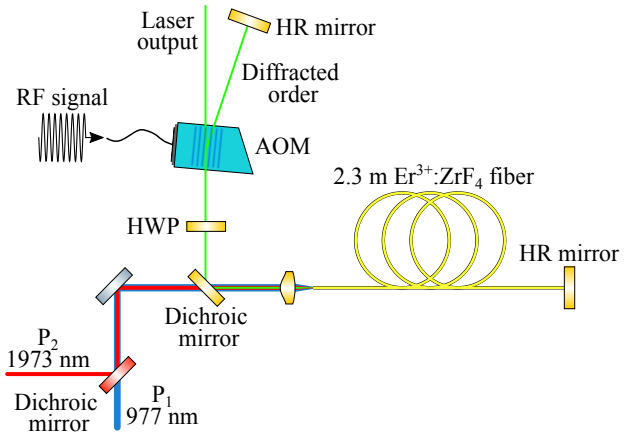

Fig. 1. Experimental setup for mode-locking experiments.

The variable frequency driver for the AOM (Gooch & Housego MVH029-031-20AS2-A1) produced RF signals in the range of 17.4 MHz to 38.3 MHz. A constant RF signal of 28.60 MHz is applied to the AOM to achieve CW lasing at 3470.4 nm. Adjusting the RF frequency provided to the AOM changes the wavelength at which the AOM exhibits its maximum diffraction efficiency, allowing to tune the wavelength of operation of the laser in both CW and mode-locking. The AOM always operates at maximum diffraction efficiency since the AOM driver does not allow changing the RF power supplied to the AOM while in continuous mode.

Rotation of the half-wave plate controls the regime of operation. Continuous wave operation is possible at low power, where the system is slightly above threshold, or with higher pump powers when the wave plate are oriented appropriately. Q-switched mode-locking and continuous wave mode-locking can also be obtained at these power levels with different orientations of the half-wave plate. At higher average output powers, only Q-switched mode-locking and continuous wave mode-locking are possible. Mode-locked operation could not be achieved without the half-wave plate. Only CW and very unstable pulsed behaviour showing telltale signs of harmonic mode-locking could be observed while the wave plate was absent. Ensuring matched polarization between the fibre output and the AOM are the likely cause as described in the next section.

B. Laser performance

Stable mode-locking laser operation is achieved once a threshold laser average power is exceeded and some experimental settings are adjusted . To achieve CW lasing minimum pump powers of 6.2 W at 977 nm and 3.1 W of the 1973 nm pump are required. The optimum orientation of the half wave plate is related to its relative direction compared with the flat surfaces on the fibre core cross-section on the AOM end of the fibre. Further discussion on the wave plate orientation is brought later in this paper. The slope efficiency of the laser in CW operation is 12% with respect to the 1973 nm pump for a fixed 980 nm pump power of 6.2 W. Once the laser is operating at power levels of about 50 mW in CW, rotating the half wave plate by 6° in either direction results in a continuous and steady train of mode-locked pulses (Fig. 2). The average power drops, however and slope efficiency reduces to 7.9%. A maximum average mode-locked output power of 367 mW is obtained for pump powers of 7.05 W and 5.67 W for the 977 nm and 1973 nm, respectively. The maximum power level is limited by the diode driver in the setup. The average output power of the laser is stable on the minute scale, however tends to drift down at longer time scales due to thermal drift associated with the voltage reference to the AOM. The laser also exhibits some variations on a microsecond timescale.

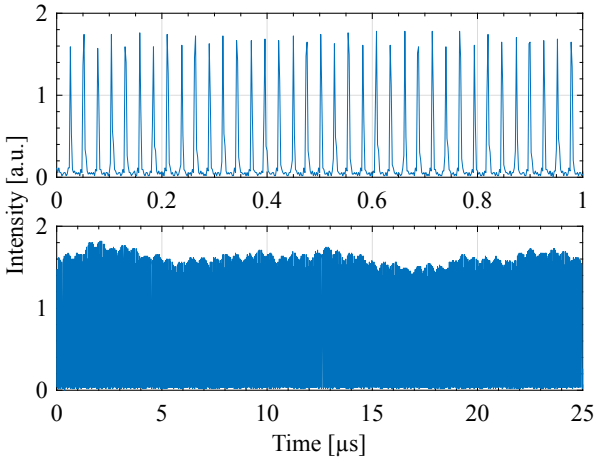

Fig. 2. Time domain output of the mode-locked laser.

A peak at the fundamental frequency of 37.75 MHz is observed when the laser output is viewed with an RF spectrum analyser (Fig. 3), connected to a fast detector (PEMI-10.6 from VIGO System). This value agrees with the inverse round trip time of the laser resonator. Sub-harmonic frequencies, 30 dB lower than the main carrier, are due to the alternating peak height of the pulses. The fundamental peak displays broad side-lobes on either side separated by approximately 100 kHz.

A two-photon absorption autocorrelation setup, similar to those used in [5], [7] was used to measure the duration of the mode-locked pulses. At the maximum available laser output power of 367 mW with the laser spectrum centred on 3472 nm, we measured pulse duration of 3.8 ps (see Fig. 4), assuming a sech^2 pulse shape. A peak power of 2.55 kW is deduced using this measurement of the pulse duration and the measured pulse energy of 9.7 nJ.

The laser output is found to be strongly polarized. When the half-wave plate is adjusted, three positions separated by $45°$ produce similar maximum power levels. In all cases the laser output is polarized very close to vertically, relative to the optical table surface. By imaging the fiber tip, this polarization plane seems to coincide with the short axis of the fiber cladding, i.e. it is perpendicular to the truncated cross-

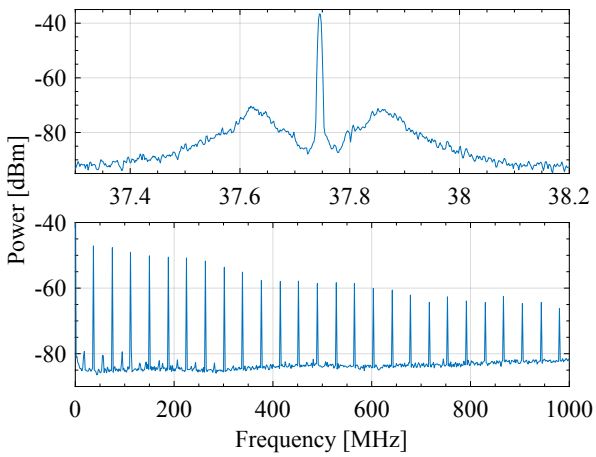

Fig. 3. Frequency spectrum of the mode-locked laser.

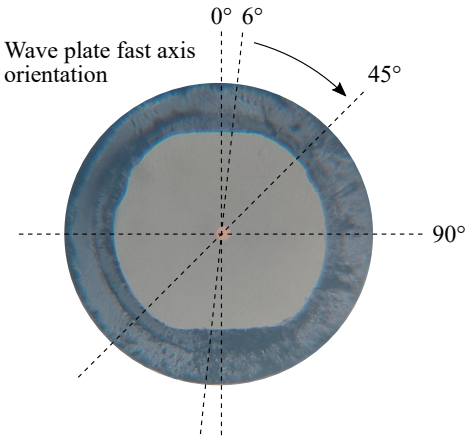

Fig. 5. Relative orientation of the half wave plate in relation to the fibre core. The offset angle to achieve mode-locking is ±6° relative to the CW orientation.

section of the fiber, see Fig. 5. A polarization extinction ratio of better than 27 dB (limited by the power meter stability) is observed when operating in CW. To obtain clean mode-locking, the wave plate position is adjusted to be ±6° off from those positions. The polarization extinction ratio in the mode-locking cases decreases to 17 dB.

The measured optical spectrum of the mode-locked laser is shown in Fig. 6. This was measured with a 0.05 nm resolution using a grating monochromator (Princeton Instruments Acton SP2500) coupled to an InSb detector (Judson Technologies J10D-M204-R04M-60). Under mode-locking conditions, the optical spectrum has a full-width, half maximum (FWHM) of 7.1 nm, centred on 3466 nm at maximum power (Fig 6 - right inset). The spectrum also exhibits strong modulation caused by amplification of etalon effects. The cause of the etalons was traced to reflections from the back surface of the HR mirror. Similar etalon effects were observed in [28] which used the same optical elements, although the cause was not known at the time. We did not observe these fluctuations in our NPR based mode-locking experiment [7] that used different optical elements. Note that the subtle high frequency shoulder in the output spectrum [25], [29], which is a feature peculiar to FSF, is not visible in the output spectrum of the current laser. The expected shoulder position at about 1 nm blue shifted from the line centre is obscured by the strong etalons.

Changing the AOM driver frequency enables electronically sweeping the central wavelength of operation whilst the laser maintains its mode-locking operation. At 60% of the maximum power while mode-locked (215 mW), the tuning range covered close to 40 nm from 3453 nm to 3490 nm, when adjusting the RF driving frequency of the AOM between 28.97 MHz and 28.50 MHz, respectively, see Fig. 7. At higher power, only slight increase of few nm in the tuning range was obtained at the longer wavelengths end. An RF driving frequency tuning rate of 12.7 kHz/nm was found. Tuning further, beyond this range was possible while the laser was operating in CW (i.e. not mode-locked) extending to a width over 50 nm. The RF

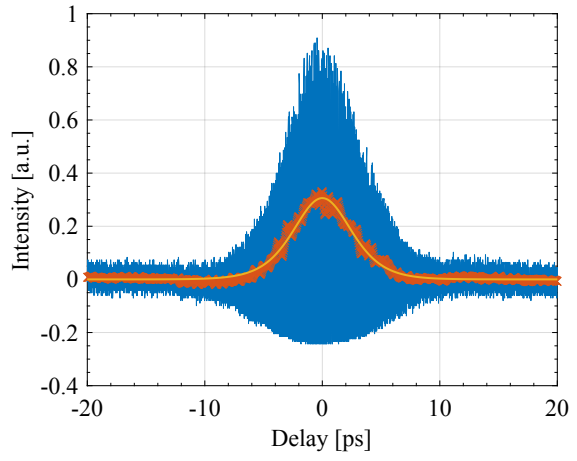

Fig. 4. Autocorrelation measurement of the mode-locked laser pulses. The resulting pulse duration is 3.8 ps for a sech^2 fit.

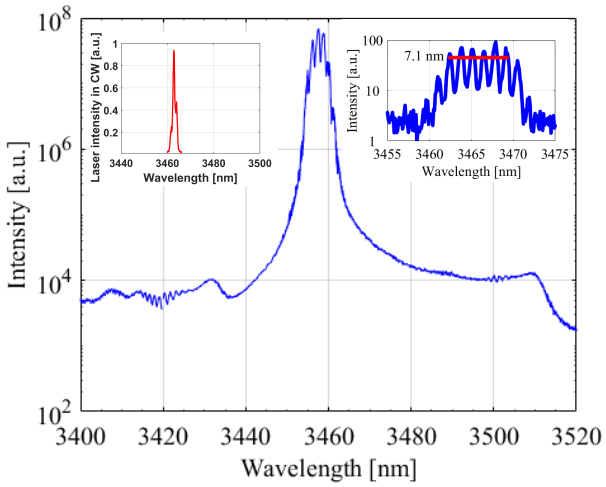

Fig. 6. Optical spectrum of the mode-locked laser observed with full dynamic range when operating at power level of 105 mW of average power. CW laser linewidth is shown for comparison (left inset). At maximum output of 367 mW, the spectral width broadens to 7.1 nm FWHM (right inset). The spectral ripple is the result of weak etalons caused by the back surface reflections from of the free space resonator mirrors.

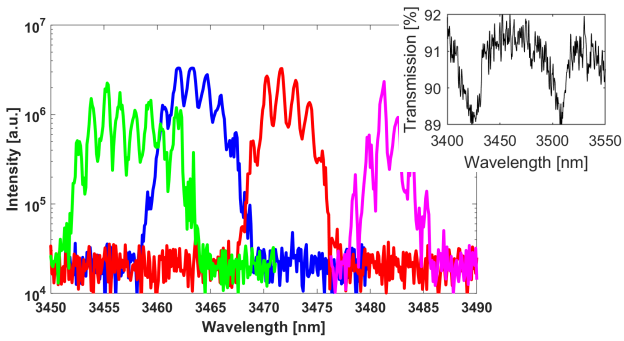

Fig. 7. Electronic wavelength tuning range while mode-locking. The tuning was achieved by adjusting the driving RF frequency between 28.97 MHz for the shortest wavelength and 28.50 MHz for the longest one. The inset shows the measured transmission curve through the AOM when it is not operating. Purging the system during the transmission measurement did not result in changes at this wavelength range.

driving frequency to wavelength tuning rate of 12.7 kHz/nm was maintained. The longest wavelength of continuous operation in CW is extended to 3501 nm. However, an additional range of operation with a few nm width was also possible at maximum power around 3520–3525 nm corresponding to the second highest peak in the Er:ZrF_4 emission cross-section and where a second independent lasing line was observed in previous works [4], [30]. Note that the AOM driving frequency was maintained close to 29 MHz throughout this work. Therefore we did not observe any potential instabilities due to driving the AOM at a frequency close to the resonator free spectral range as was observed by Majewski in [16]. The ability to electronically sweep the wavelength of operation is utilized to characterize mid-IR FBGs, as will be discussed later in this paper.

III. Discussion

The pulse duration of 3.8 ps demonstrated here lies between the ultra-fast pulses of 580 fs demonstrated in [7] using NPR and the long pulses of 53 ps achieved using FSF with an AOTF [5]. Our results are also significantly shorter than pulse durations of 20 ps reported by by Majewski et al. [17] using a very similar laser architecture on the 2.8 µm erbium transition. Our result support the hypothesis proposed by Majewski et al. [17] that operating in a water vapor free window will allow shorter duration. Although our current implementation did not allow sub picosecond pulse durations to be achieved, unlike the 825 fs pulse duration inferred in Majewski's same work that used the same AOM setup but with a dysprosium fiber. This is likely due to the combination of the cross section of this laser transition being low (relatively to other mid-IR transitions [31]) compounded by the AOM's bandpass having variations and losses in the AOM optical coating, which is optimized for the 3 µm range.

In our NPR experiment [7] the setup benefited from both unrestricted spectral bandwidth (except the coating on the optics) in addition to very low absorption of water vapour at this band. Hence sub-picosecond pulses were possible. Other works, on the 2.8 µm erbium transition showed that NPR resonators produces pulses with hundreds of femtosecond duration despite the atmospheric absorption [32] [33], This is potentially due to the higher peak power of the pulses effectively saturating the water transition but note that water absorption lines are still imprinted onto the laser spectrum.

CW operation was achieved rather easily with our set-up. We attribute this to larger bandwidth of the AOM compared with the AOTF and lack of atmospheric absorption at 3.5 µm, in contrast to Majewski's work [17]. The frequency shifting per round trip is small enough to allow multiple amplification rounds while remaining within the bandwidth of the AOM. An open question that remains to be answered is the spectral filtering mechanism that enables the short pulse operation using an AOM. In the case of an AOTF design, there is a clear spectral filtering effect which is thought to be necessary to favour short pulsing. The AOM presents a considerably broader optical bandwidth and currently the exact spectral filtering mechanism is unknown.

We hypothesize that spectral filtering is present but to a significantly lesser extent than present with the AOTF. Operating at moderate power levels not far above threshold power and in CW mode demonstrated clear dependency on the exact frequency of the AOM drive. Distinctive side-lobes ripple in the behaviour of the AOM was observed with the voltage tuning of the AOM. An optimum driving frequency is found where it is necessary to be within ± 2.5 kHz, (equivalent to ± 0.2 nm) to reach lasing or obtain higher operating power when further from the threshold. Once operating sufficiently above threshold, this behaviour repeated itself every shift of ± 67.3 kHz, which is equivalent to 5.3 nm between peaks, however the measured laser power at every successive side-lobe is reduced further compared with the optimum wavelength.

Multiple side lobes on both sides of the optimum could be found, each one of about 7 kHz width and with successively lower laser power. The gap between the successive side-lobes does not match the etalons, so it is presumed to be related to narrow artifacts of the transmission of the AOM potentially obscured by the noise in the transmission curve shown in the inset of Fig. 7. We expect that a higher gain laser transition would have been much less susceptible to these variations in the resonator loss. On the other hand, the strong reliance on reduced loss is likely to be the mechanism providing the spectral filtering necessary to achieve mode-locked behaviour.

The optical spectrum of Fig. 6 does not contain any indication to Kelly sidebands, unlike the case in Majewski's experiment using the AOM at 2.9 µm with Dy^{3+} doped ZBLAN. Observing the spectrum over wider spans did not change this observation. The time-bandwidth product of the pulses at maximum power is 0.67. The pulses are therefore significantly chirped providing additional indication that there are no solitons involved.

As a further check, we can also use the soliton area theorem,

$$E_{\mathrm{p}} = \frac{2|\beta_2|}{|\gamma|\tau},$$

where E_{p} is the pulse energy and the FWHM pulse duration is 1.763τ. Values for group velocity dispersion $\beta_2 = -0.191 \times 10^{-24}\,\mathrm{s^2 m^{-1}}$ and self-phase modulation constant $\gamma = 0.83 \times 10^{-4}\,\mathrm{W^{-1} m^{-1}}$ can be found in [7]. Using the

experimentally determined pulse duration, the soliton area theorem gives a pulse energy that is thirteen times smaller than the measured value after accounting for the measured 60% diffraction efficiency and 91% transmission of the AOM at 3.47 µm, providing further evidence of the lack of solitonic action. Overall, the peak power of 2.55 kW is not high enough to invoke sufficient Kerr nonlinearity which means true conservative solitons do not form. This is indicated by the large time-bandwidth product, the lack of Kelly sidebands in the spectrum and the large pulse energy in relation to the pulse energy expected from a soliton.

The lack of solitonic action is not unusual for FSF based mode-locking lasing as was suggested by Majewski, where their appearance in his instance was considered unusual, since Kelly side bands have only been observe in NPR-based mode-locked instances.

IV. FBG INTERROGATION

Methods for characterising FBGs and FBG arrays in the near-IR have been available for over two decades driven by needs of modern fiber-optic based telecommunication systems [34]. Three main approaches are used in this space to determine the spectral properties of FBGs: Using a broadband source with a narrow linewidth filtered sensor on the detection side, for example a supercontinuum source with a diffraction grating based detector. The second option is to use a multitude of narrow band fixed wavelength switched sources, this approach is mostly useful for arrays of predefined wavelength FBG, as in the standard telecom wavelength grid. Lastly, a tunable narrow linewidth source that can be used while it is synchronized to the detection side of the system. [34]

Mid-IR FBGs for wavelengths beyond 3 µm remain difficult to produce reliably and fabrication is limited to only a handful of research labs [2], [35], [36]. Initially the method of writing the refractive index change in the fiber was based on using the phase-mask method in ZBLAN [35], however in recent years alternative writing methods using the point-by-point method as demonstrated by Bharatan [36] and then the plane-by-plane method as was first shown by Goya are starting to be used. These new methods allow for significant flexibility in the FBG parameters including obtaining chirping more easily [37] and tilting of the FBG [38]. The flexibility and relative ease of creating complex structures using a mask-less method enabled for example the creation of tilted-FBGs in fibers [38] and waveguide structure in bulk ZBLAN glass [39]. As a key enabler for the rapid development of point-by-point and plane-by-plane FBGs, a rapid method for testing the reflectivity of an FBGs is necessary. We therefore propose to use the aforementioned electronically swept source demonstrated previously and utilize it to interrogate mid-IR FBGs.

The electronically wavelength swept beam is used as a mid-IR FBG interrogator, as a first proof of concept to the best of our knowledge. We investigated the spectral properties of a mid-IR FBG fabricated into a fiber with a 16.5 µm core using the plane-by-plane femtosecond laser inscription method [40]–[42]. The femtosecond laser system (HighQ laser femtoREGEN) operated at 517 nm with a pulse duration of

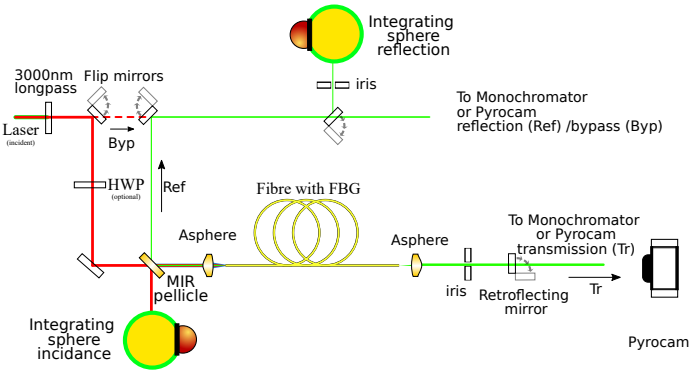

Fig. 8. Setup used for the characterisation of mid-IR FBGs inscribed in the ZrF_4 fiber.

220 fs. For the inscription, the repetition rate of the laser was set at 10 kHz with a pulse energy at 250 nJ. The laser beam was focused through the protective cladding layer of the fiber into its core using a long working distance ($\times 50$) microscope objective with a 0.4 NA The fibre samples were mounted on an air-bearing translation stage (Aerotech) for a two-axis nanometre accuracy movement during the inscription process, while a third manual stage was used for the alignment of the focus distance. The FBGs were second order gratings with a length of 12 mm and pitch period of 2.33 µm.

The FBG interrogator used our laser in CW mode which was achieved by rotating the intracavity half-wave plate for CW operation as discussed previously . The 3.5 µm laser was wavelength swept between 3450 nm and 3497 nm by applying a triangle ramp voltage pulse train to the AOM driver, resulting in a wavelength sweep.

A schematic of the FBG interrogator is shown in Fig. 8. Light from the laser is incident on a mid-IR pellicle beam splitter (Thorlabs BP145B4). The transmitted beam is used to measure the incident power, by detecting it with a PbSe detector (Thorlabs PDA20H) coupled to an integrating sphere (Newport 3P-GPS-030-IG). The power reflected from the pellicle beam splitter is launched by a custom aspheric lens into the FBG containing fibre. Light that bypasses the FBG in the core will not properly reflect backwards (due to angle on the distal end of the fibre) and will not be recorded by the detectors on the reflection arm, discussed thereafter. In most cases both ends of the fiber are Brewster angle polished to prevent the Fresnel reflection dominating the reflection signal, while in some cases the distal end is flat polished to use the Fresnel reflection as a reference. Great care is taken to ensure the laser beam is launched into the core so that it interacts with the FBG and does not bypass it, as happens very easily in double clad fibers.

The emerging beam is sent to additional diagnostic equipment consisting of a power meter, grating monochromator, and a thermopile-based laser beam diagnostic camera. A retroflecting mirror after the collimator is used to launch the beam back through the fiber core for alignment and to calibrate the reflected power reading on the oscilloscope. The part of the beam reflected by the FBG is partially reflected by the pellicle into the same diagnostic equipment. A flip mirror diverts the

beam into an identical PbSe detector and integrating sphere combination; both detectors are connected to an oscilloscope. The AOM driver voltage is ramp swept at 77 Hz, causing the laser wavelength to scan across the reflection band of the FBG. Scanning at much higher frequencies, up to a few kHz was also trialed but resulted in a much worse signal to noise. The main limitation on the sweep frequency at this repetition rate is the stability of the laser output on short time scale sweeping, likely to be dependant on the inverse of the upper lasing level lifetime (160–120 µs [43]). Initial measurements calibrate the driver voltage to a wavelength span using the monochromator, mapping the oscilloscope time base position to wavelength. The reading on the reflection arm detector is normalized by the incident detector reading.

Figure 9a shows an absolute reflection curve of the FBG inscribed into the fiber. Absolute FBG reflectivity can be inferred to within 10% using the retroflecting mirror, with the FBG curve shown here corresponding to a 30% peak reflectivity. In cases where the signal to noise is high, it is also possible to use the flat Fresnel reflection of the distal end as a 3.6% reflective reference with better absolute results. Testing this method using a double-clad fiber is challenging compared with a single clad fiber. It is essential to ensure that the swept beam is well coupled into the core and does not bypass the FBG by propagating in the cladding. This delicate process of alignment was achieved by adjusting the coupling mirrors while monitoring the output while interchanging the power meter and camera.

In the current configuration the laser's CW linewidth of 0.95 nm (see Fig. 9c) is wider than desired for an interrogator configuration. The reflected signal captured by the PbSe detectors as seen in Fig. 9b has no spectral filtering. Therefore, the signal is a convolution of the FBG spectral response together with the spectral shape of the incoming wavelength swept beam, with a typical lineshape seen in Fig. 9c and represented numerically by the Equation:

$$Laser(\Delta\lambda') * FBG(\Delta\lambda') = \int_{-\infty}^{\infty} Laser(\Delta\lambda) FBG(\lambda' - \Delta\lambda) d\lambda'$$

with $Laser(\Delta\lambda')$ and $FBG(\Delta\lambda')$ representing the laser and the FBG's linewidth, respectively. To account for this effect, after translating the recorded oscilloscope signal to its equivalent wavelength range, it is de-convoluted using the "deconvblind" Matlab™ algorithm [44] using the recorded spectral shape of the laser in CW when the laser is not swept. We verified that the spectral shape of the incident beam does not change substantially within the swept range. An example of the difference between the raw and deconvolved FBG lineshapes is shown in Fig. 9d. In addition, the incident power was continuously monitored and the transmission or reflection through the FBG are referenced in real time to the incident swept signal.

For a wide FBG, with spectral width greater than a few nanometers, a transmission measurement using a technique similar to the deconvolution method described above is possible. For narrow FBGs, the transmission dip of the FBG is lost due to the relatively broad spectral linewidth of the laser and as a result the deconvolution method did not work. To circumvent this and measure narrow FBG transmission we continuously swept the laser wavelength and then passed the transmitted light into a spectrometer. The transmission profile was obtained by holding the spectrometer at a particular wavelength and the max hold function was used to retain the highest transmitted light. The spectrometer was then stepped to the next wavelength position and this was repeated until the transmission profile was obtained. Our setup did not allow for an effective reference to measure the transmitted beam power fraction while using the spectrometer. Therefore, the transmission curve shown in Fig. 9a provides only qualitative information on the location of the transmission notch. Future implementation of this setup will address this point.

An effective dynamic range of about 25 dB in the reflectivity measurement is seen in Fig. 9. Better dynamic range can be achieved by increasing the laser power incident on the fiber, or using a pair of detectors with higher gain that can lift smaller signals further above the noise floor of the oscilloscope compared with the fixed gain of the PbSe detectors used.

Out of band loss is also an important parameter that is usually measured in transmission mode. In our case, it is measured to be 2 dB at 3470 nm. We measure the out of band transmission loss by comparing the transmitted power through the fiber with the FBG when the laser is operated at a wavelength removed from the wavelength of the FBG. We then compare the transmitted power with a similar fiber without an inscribed FBG.

The wavelength tuning range appears to be limited by the currently available pump power. This is due to the diffraction angle changing slightly with the shift in the laser wavelength. Therefore, the beam that is reflected back by the HR mirror cannot retrace its way back into the core of the gain fiber precisely, resulting with increased losses at the demonstrated tuning range. The tuning range observed conforms with ±25 nm around the peak of the emission cross-section curve of the 3.5 µm transition [28]. Using as a basis for comparison the numerical analysis of a 2.4 m resonator with two butted mirrors [18], [31], [45] suggests that additional 53% of additional round-trip losses are required to reproduce the observed average power level measured experimentally in this configuration compared with a simple resonator with a fibre butted against two mirrors. The additional loss is coming from the non-optimal coating on the AOM and losses due to collimating and launching back into the fibre core.

V. Conclusion

We have demonstrated a mode-locked fiber laser operating at the 3.5 µm range with 3.8 ps pulse duration by using the DWP method in Er^{3+}:ZrF_4. The mode-lockig is created by using an AOM implementing the frequency-shifted feedback method. The significantly reduced pulse duration at the water vapor free, 3.5 µm band compared with a similar AOTF-based system confirms the assertion that the longer pulse duration in the AOTF case is the result of the spectral filtering caused by its limited passband compared with an AOM.

A factor of 14 reduction in pulse width was obtained. However, although the 3.5 µm band is significantly less sus-

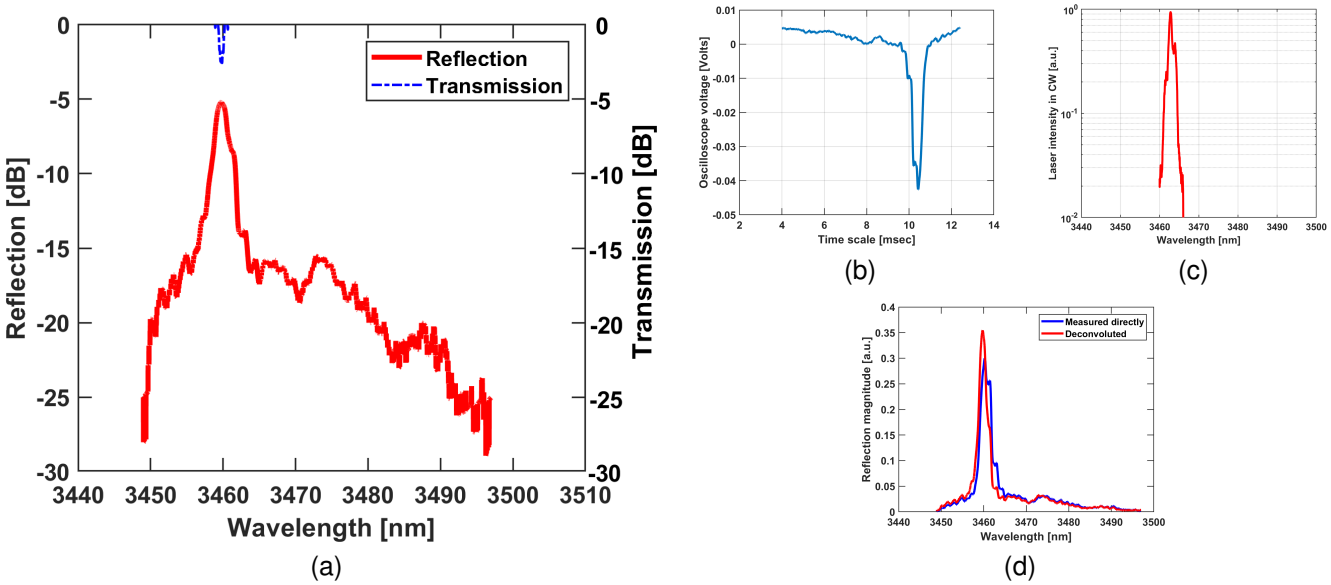

Fig. 9. (a) Reflectivity and transmission of the FBG under test. The reflectivity was measured using the swept source with the experimental setup shown in Fig. 8. The transmission spectrum was determined using the monochromator while sweeping the source and looking for the maximum transmission as a function of wavelength. (b) Raw Oscilloscope trace as a function of time, measured with the PbSe detectors. (c) Typical spectral lineshape of laser in CW mode. (d) Difference in FBG shape between raw measurement and deconvolved shape based on the incident lineshape.

ceptible to atmospheric absorption, ultrafast, sub-picosecond pulse duration was not achieved using an AOM at 3.5 µm due to a combination of restrictions in the AOM, optics and the lower gain of this transition. This is in contrast to previous demonstration of AOM-based FSF at the 3 µm range.

We used the same laser system as an electronically swept mid-IR FBG interrogator when operating below mode-locking threshold. Although the laser linewidth imposed some limitations, this is the first proof-of-concept of a an electronically swept interrogator in the mid-IR, to the best of our knowledge. The swept source was used to characterize a sample of mid-IR FBGs in a double clad fiber at the 3.5 µm band. Improved performance and better characterisation capabilities will be the focus of future work.

ACKNOWLEDGMENT

This work was supported in part by the US Air Force Office of Scientific Research award FA-9550-20-1-0160, Australian Research Council project DP210102442, the University of Adelaide and the European Regional Development Fund and the Republic of Cyprus through the Research and Innovation Foundation (Project: POST-DOC/0718(sp. ext.)/0003). This work was performed, in part, at the Opto Fab node of the Australian National Fabrication Facility supported by the Commonwealth and SA State Government. This work was supported by and in part performed at the Cyprus University of Technology.

REFERENCES

[1] F. Adler, P. Masłowski, A. Foltynowicz, K. C. Cossel, T. C. Briles, I. Hartl, and J. Ye, "Mid-infrared fourier transform spectroscopy with a broadband frequency comb," *Optics express*, vol. 18, no. 21, pp. 21 861–21 872, 2010.

[2] M. R. Majewski, G. Bharathan, A. Fuerbach, and S. D. Jackson, "Long wavelength operation of a dysprosium fiber laser for polymer processing," *Optics Letters*, vol. 46, no. 3, pp. 600–603, 2021.

[3] M. Winkowski and T. Stacewicz, "Optical detection of formaldehyde in air in the 3.6 µm range," *Biomedical Optics Express*, vol. 11, no. 12, pp. 7019–7031, 2020.

[4] O. Henderson-Sapir, J. Munch, and D. J. Ottaway, "Mid-infrared fiber lasers at and beyond 3.5 µm using dual-wavelength pumping," *Optics Letters*, vol. 39, no. 3, pp. 493–496, 2014.

[5] O. Henderson-Sapir, N. Bawden, M. R. Majewski, R. I. Woodward, D. J. Ottaway, and S. D. Jackson, "Mode-locked and tunable fiber laser at the 3.5 µm band using frequency-shifted feedback," *Optics Letters*, vol. 45, no. 1, pp. 224–227, 2020.

[6] Z. Qin, T. Hai, G. Xie, J. Ma, P. Yuan, L. Qian, L. Li, L. Zhao, and D. Shen, "Black phosphorus Q-switched and mode-locked mid-infrared Er:ZBLAN fiber laser at 3.5 µm wavelength," *Optics Express*, vol. 26, no. 7, p. 8224, Apr. 2018.

[7] N. Bawden, O. Henderson-Sapir, S. D. Jackson, and D. J. Ottaway, "Ultrafast 3.5 µm fiber laser," *Optics Letters*, vol. 46, no. 7, pp. 1636–1639, 2021.

[8] J. Wei, P. Li, L. Yu, S. Ruan, K. Li, P. Yan, J. Wang, J. Wang, C. Guo, W. Liu, P. Hua, and Q. Lü, "Mode-locked fiber laser of 3.5 µm using a single-walled carbon nanotube saturable absorber mirror," *Chinese Optics Letters*, vol. 20, no. 1, p. 011404, 2022.

[9] T. Hai, G. Xie, J. Ma, H. Shao, Z. Qiao, Z. Qin, Y. Sun, F. Wang, P. Yuan, J. Ma, and L. Qian, "Pushing optical switch into deep mid-infrared region: Band theory, characterization, and performance of topological semimetal antimonene," *ACS Nano*, vol. 15, no. 4, pp. 7430–7438, 2021.

[10] H. Luo, J. Yang, J. Li, and Y. Liu, "Widely tunable passively Q-switched Er^{3+}-doped ZrF_4 fiber laser in the range of 3.4 µm based on a Fe^{2+}:ZnSe crystal," *Photonics Research*, vol. 7, no. 9, pp. 1106–1111, 2019.

[11] Z. Fang, C. Zhang, J. Liu, Y. Chen, and D. Fan, "3.46 µm Q-switched Er^{3+}:ZBLAN fiber laser based on a semiconductor saturable absorber mirror," *Optics & Laser Technology*, vol. 141, p. 107131, 2021.

[12] Z. Qin, Y. Zhou, G. Xie, P. Yuan, J. Ma, and L. Qian, "Red-diode-clad-pumped CW and mode-locked Er:ZBLAN fiber laser at 3.5 µm," *Optics Express*, vol. 30, no. 7, pp. 11 174–11 180, 2022.

[13] Z. Qin, X. Chai, G. Xie, Z. Xu, Y. Zhou, Q. Wu, J. Li, Z. Wang, Y. Weng, T. Hai, P. Yuan, J. Ma, J. Chen, and L. Qian, "Semiconductor saturable absorber mirror in the 3–5 µm mid-infrared region," *Optics Letters*, vol. 47, no. 4, pp. 890–893, 2022.

[14] A. Malouf, O. Henderson-Sapir, S. Set, S. Yamashita, and D. J. Ott-

away, "Two-photon absorption and saturable absorption of mid-IR in graphene," *Applied Physics Letters*, vol. 114, no. 9, p. 091111, 2019.
[15] V. B. Voloshinov, "Close to collinear acousto-optical interaction in paratellurite," *Optical Engineering*, vol. 31, no. 10, pp. 2089–2094, 1992.
[16] M. R. Majewski, R. I. Woodward, and S. D. Jackson, "Ultrafast mid-infrared fiber laser mode-locked using frequency-shifted feedback," *Optics Letters*, vol. 44, no. 7, pp. 1698–1701, 2019.
[17] M. R. Majewski, M. Pawliszewska, and S. D. Jackson, "Picosecond pulse formation in the presence of atmospheric absorption," *Optics Express*, vol. 29, no. 12, pp. 19 159–19 169, 2021.
[18] N. Bawden, H. Matsukuma, O. Henderson-Sapir, E. Klantsataya, S. Tokita, and D. J. Ottaway, "Actively Q-switched dual-wavelength pumped Er^{3+}:ZBLAN fiber laser at 3.47 µm," *Optics letters*, vol. 43, no. 11, pp. 2724–2727, 2018.
[19] N. Bawden, O. Henderson-Sapir, M. R. Majewski, R. I. Woodward, S. D. Jackson, and D. J. Ottaway, "Q-switched and mode-locked 3.5 µm fiber laser," in *14th Pacific Rim Conference on Lasers and Electro-Optics (CLEO PR 2020)*, ser. OSA Technical Digest. Optica Publishing Group, Conference Proceedings, p. C3A_3.
[20] R. I. Woodward, M. R. Majewski, D. D. Hudson, and S. D. Jackson, "Swept-wavelength mid-infrared fiber laser for real-time ammonia gas sensing," *APL Photonics*, vol. 4, no. 2, p. 020801, 2019.
[21] J.-P. Bérubé, C. Frayssinous, J. Lapointe, S. Duval, V. Fortin, and R. Vallée, "Direct inscription of on-surface waveguides in polymers using a mid-IR fiber laser," *Optics Express*, vol. 27, no. 21, pp. 31 013–31 022, 2019.
[22] M. J. Baker, J. Trevisan, P. Bassan, R. Bhargava, H. J. Butler, K. M. Dorling, P. R. Fielden, S. W. Fogarty, N. J. Fullwood, K. A. Heys, C. Hughes, P. Lasch, P. L. Martin-Hirsch, B. Obinaju, G. D. Sockalingum, J. Sulé-Suso, R. J. Strong, M. J. Walsh, B. R. Wood, P. Gardner, and F. L. Martin, "Using fourier transform ir spectroscopy to analyze biological materials," *Nature Protocols*, vol. 9, no. 8, pp. 1771–1791, 2014.
[23] O. A. Romanovskii, S. A. Sadovnikov, O. V. Kharchenko, and S. V. Yakovlev, "Development of near/mid IR differential absorption opo lidar system for sensing of atmospheric gases," *Optics & Laser Technology*, vol. 116, pp. 43–47, 2019.
[24] C. Li, L. Dong, C. Zheng, J. Lin, Y. Wang, and F. K. Tittel, "Ppbv-level ethane detection using quartz-enhanced photoacoustic spectroscopy with a continuous-wave, room temperature interband cascade laser," *Sensors*, vol. 18, no. 3, p. 723, 2018.
[25] R. I. Woodward, M. R. Majewski, and S. D. Jackson, "Mode-locked dysprosium fiber laser: Picosecond pulse generation from 2.97 to 3.30 µm," *APL Photonics*, vol. 3, no. 11, p. 116106, 2018.
[26] H. Sabert and E. Brinkmeyer, "Pulse generation in fiber lasers with frequency shifted feedback," *Journal of Lightwave Technology*, vol. 12, no. 8, pp. 1360–1368, 1994.
[27] I. C. M. Littler, S. Balle, and K. Bergmann, "Continuous-wave laser without frequency-domain-mode structure: investigation of emission properties and buildup dynamics," *Journal of the Optical Society of America B*, vol. 8, no. 7, pp. 1412–1420, 1991.
[28] O. Henderson-Sapir, S. D. Jackson, and D. J. Ottaway, "Versatile and widely tunable mid-infrared erbium doped ZBLAN fiber laser," *Optics Letters*, vol. 41, no. 7, p. 1676, Apr. 2016.
[29] O. Henderson-Sapir, N. Bawden, M. R. Majewski, R. I. Woodward, D. J. Ottaway, and S. D. Jackson, "Mode-locked and tunable fiber laser at the 3.5 µm band using frequency-shifted feedback," *Optics Letters*, vol. 45, no. 1, p. 224, Jan. 2020.
[30] M. J. Henderson-Sapir O., Ottaway D. J., "Mid-infrared 3.5 µm band Er^{3+}:ZBLAN fibre laser," 2014.
[31] O. Henderson-Sapir, A. Malouf, N. Bawden, J. Munch, S. D. Jackson, and D. J. Ottaway, "Recent advances in 3.5 µm erbium-doped mid-infrared fiber lasers," *IEEE Journal of Selected Topics in Quantum Electronics*, vol. 23, no. 3, pp. 1–9, 2017.
[32] S. Duval, M. Bernier, V. Fortin, J. Genest, M. Piché, and R. Vallée, "Femtosecond fiber lasers reach the mid-infrared," *Optica*, vol. 2, no. 7, pp. 623–626, 2015.
[33] L. Yu, J. Liang, S. Huang, J. Wang, J. Wang, X. Luo, P. Yan, F. Dong, X. Liu, Q. Lue, C. Guo, and S. Ruan, "Average-power (4.13 w) 59 fs mid-infrared pulses from a fluoride fiber laser system," *Optics Letters*, vol. 47, no. 10, pp. 2562–2565, May 2022.
[34] R. Nabiev and W. Yuen, "Tunable lasers for multichannel fiber-optic sensors: tunable lasers, highly manufacturable and cost-effective, are opening new opportunities for multichannel fiber bragg grating sensors using single-fiber and single-laser technology in multiple-point interrogation systems," *Sensors Magazine*, vol. 20, no. 8, pp. 28+, 2003/08// 2003.
[35] V. Fortin, F. Maes, M. Bernier, S. T. Bah, M. D'Auteuil, and R. Vallée, "Watt-level erbium-doped all-fiber laser at 3.44 µm," *Optics Letters*, vol. 41, no. 3, pp. 559–562, 2016.
[36] G. Bharathan, T. T. Fernandez, M. Ams, J.-Y. Carrée, S. Poulain, M. Poulain, and A. Fuerbach, "Femtosecond laser direct-written fiber bragg gratings with high reflectivity and low loss at wavelengths beyond 4 µm," *Optics Letters*, vol. 45, no. 15, pp. 4316–4319, 2020.
[37] A. Fuerbach, G. Bharathan, S. Antipov, M. Ams, R. Williams, D. Hudson, R. Woodward, and S. Jackson, "Line-by-line femtosecond FBG inscription for innovative fiber lasers," in *Bragg Gratings, Photosensitivity and Poling in Glass Waveguides and Materials*. Optical Society of America, 2018, Conference Proceedings, p. BW3A. 6.
[38] G. Bharathan, D. D. Hudson, R. I. Woodward, S. D. Jackson, and A. Fuerbach, "In-fiber polarizer based on a 45-degree tilted fluoride fiber bragg grating for mid-infrared fiber laser technology," *OSA Continuum*, vol. 1, no. 1, pp. 56–63, 2018.
[39] O. Henderson-Sapir, S. O. Fashola, N. Bawden, A. Dowler, A. Ng, D. J. Ottaway, A. Fuerbach, and H. Ebendorf-Heidepriem, "Mid-infrared Er^{3+} : ZBLAN waveguide using ZBLAN glass extrusion, femtosecond inscription and dual-wavelength pumping for the generation of 3.5 µm lasing," in *2020 22nd International Conference on Transparent Optical Networks (ICTON)*, 2020, Conference Proceedings, pp. 1–4.
[40] A. Theodosiou, A. Lacraz, M. Polis, K. Kalli, M. Tsangari, A. Stassis, and M. Komodromos, "Modified fs-laser inscribed FBG array for rapid mode shape capture of free-free vibrating beams," *IEEE Photonics Technology Letters*, vol. 28, no. 14, pp. 1509–1512, 2016.
[41] A. Theodosiou, A. Lacraz, A. Stassis, C. Koutsides, M. Komodromos, and K. Kalli, "Plane-by-plane femtosecond laser inscription method for single-peak bragg gratings in multimode cytop polymer optical fiber," *Journal of Lightwave Technology*, vol. 35, no. 24, pp. 5404–5410, 2017.
[42] A. Ioannou, A. Theodosiou, C. Caucheteur, and K. Kalli, "Direct writing of plane-by-plane tilted fiber bragg gratings using a femtosecond laser," *Optics Letters*, vol. 42, no. 24, pp. 5198–5201, 2017.
[43] O. Henderson-Sapir, J. Munch, and D. J. Ottaway, "New energy-transfer upconversion process in Er^{3+}:ZBLAN mid-infrared fiber lasers," *Optics Express*, vol. 24, no. 7, pp. 6869–6883, 2016.
[44] D. S. C. Biggs and M. Andrews, "Acceleration of iterative image restoration algorithms," *Applied Optics*, vol. 36, no. 8, pp. 1766–1775, 1997.
[45] A. Malouf, O. Henderson-Sapir, M. Gorjan, and D. J. Ottaway, "Numerical modeling of 3.5 µm dual-wavelength pumped erbium-doped mid-infrared fiber lasers," *IEEE Journal of Quantum Electronics*, vol. 52, no. 11, pp. 1–12, Nov. 2016.

Ori Henderson-Sapir received the B.Sc. degree in physics and mathematics from Hebrew University, Jerusalem, Israel, and the M.Eng. degree from Tel-Aviv University, Tel Aviv, Israel, where he worked on the development of electrically small antennas. He received the Ph.D. degree from the University of Adelaide, Adelaide, SA, Australia with the Lasers and Optics Group working on the development of mid-infrared fiber optic lasers. Ori then divided his time as an Optics and Laser Engineer at Ellex Medical and as a Research Associate at the University of Adelaide continuing his work with mid-infrared fiber lasers. He later joined the Precision Measurement Group at the Institute for Photonics and Advances Sensing (IPAS) working on the cryogenic sapphire oscillators ultra-stable clocks, while he continued developing fiber laser as well. He recently returned to work exclusively on mid-infrared fiber lasers and sensing applications focusing on tunable, mode-locked and high-power mid infrared fiber lasers. Ori is the founder and CEO of Mirage Photonics a mid-infrared fiber laser start-up.

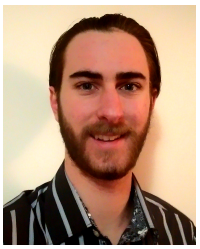

Nathaniel Bawden received his B.Sc. (Hons.) degree in physics from The University of Adelaide in 2016. He received the Ph.D. degree from The University of Adelaide in 2021 for his dissertation on pulsed mid-infrared fiber lasers. In 2022, he joined the Quantum Optics Lab at The University of Queensland as a post-doctoral research fellow.

Antreas Theodosiou Dr. Antreas Theodosiou is the director and founder of the Lumoscribe LTD. He received the B.Sc. degree in electrical engineering and the M.Sc. degree in electrical engineering, with specialization in communication systems from Frederick University, Cyprus, in 2011 and 2013, respectively, and the Ph.D. degree, with specialization in photonics and optical sensing, from the Cyprus University of Technology in 2018. He is currently part of the Photonics and Optical Sensors Laboratory (PhOSLab) in Cyprus University of Technology and the Photonics Research Center (PRC). His research includes inscription and development of optical sensors using femtosecond laser systems, waveguides, Bragg gratings, Mach-Zehnders, Fabry-Perot cavities, in polymer, silica, and other novel optical materials, and various applications using optical fibre sensors In addition, Dr. Theodosiou is experienced working with demodulation algorithms for complicated Bragg gratings spectrums, and fibre lasers.

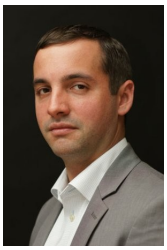

Matthew R. Majewski Matthew R. Majewski received a MS from Northeastern University in 2012. Prior to joining Macquarie University in 2014 he was member of the high power laser development team at Silex Systems (Australia). He completed his PhD thesis on dysprosium mid-infrared fiber lasers in 2017 and subsequently joined the Mid-infrared Fiber Sources Group as a research fellow. His current research focus is the development of novel high power and ultrafast fiber laser sources.

Kyriacos Kalli heads the Photonics and Optical Sensors Research Laboratory at the Cyprus University of Technology. He received the B.Sc. degree in theoretical physics and the Ph.D. degree in physics from the University of Kent, U.K., in 1988 and 1992, respectively, where he studied linear and nonlinear phenomena in optical fibers. He joined the Cyprus University of Technology (CUT) in 2008. He is currently on the Board of Directors of the Cyprus Organization for Standardization. He is also a Professor with the Department of Electrical Engineering, Computer Engineering and Informatics. He is also the Director of the Photonics and Optical Sensors Research Laboratory and runs the Femtosecond Laser Foundry. He has more than 230 journal and conference publications. He is the coauthor of Fiber Bragg Gratings: Fundamentals and Applications in Telecommunications and Sensing. His research interests are in Bragg grating and optical fiber sensors, femtosecond laser micro-fabrication of photonic devices, microfluidics, and plasmonics. He is a member of the Institute of Physics, is a Chartered Physicist, a member of the IEEE and senior member of the OSA.

Stuart D. Jackson is a Professor at the Department of Engineering at Macquarie University. He received the BSc(Hons) degree in 1989 from the University of Newcastle (Australia). In 1990, he joined the Centre for Lasers and Applications at Macquarie University to undertake research toward the PhD degree. In 1995, he joined the Laser Photonics Group at the University of Manchester and initiated the research there into high power fiber lasers. Later in 1999, he returned to Australia and joined the Optical Fiber Technology Centre (OFTC) at the University of Sydney where he became a Senior Research Fellow and technical manager of silicate fiber fabrication. During this time, he received an Australian Research Fellowship from the Australian Research Council (ARC). In 2009, he joined the School of Physics at the University of Sydney as a Queen Elizabeth II Fellow (ARC) where he became the Leader of the Flagship Project "Mid-infrared Photonics" within the ARC Centre of Excellence funded Centre for Ultrahigh-bandwidth Devices for Optical Systems (CUDOS). In early 2014, he moved to the Department of Engineering at Macquarie University to take up a permanent position in teaching and optical and photonics engineering research.

David J. Ottaway received the Ph.D. degree from The University of Adelaide, in 1999. His Ph.D. dissertation was on solid state laser sources for gravitational wave detection. In 2000, he joined the LIGO Laboratory, first as a Post-Doctoral Scholar at the LIGO Hanford Observatory, Richland, Washington, and later as a Staff Scientist with the Massachusetts Institute of Technology. During this period, he conducted research on commissioning the Initial LIGO detectors and developing optical and mechanical systems for the advanced LIGO detectors. In 2007, returned to The University of Adelaide, where he continues to develop laser and optical systems for advanced gravitational wave detectors and other forms of extreme remote sensing, including remote trace gas detection and atmospheric temperature studies.